Practical Analytical Model and Comprehensive Comparison of Power Loss Performance for Various MMCs Based on IGCT in HVDC Application

Biao Zhao⬮, *Member, IEEE*, Rong Zeng⬮, *Senior Member, IEEE*, Jianguo Li, Tianyu Wei⬮, Zhengyu Chen, Qiang Song⬮, *Member, IEEE*, and Zhanqing Yu⬮, *Member, IEEE*

Abstract—**This paper gives a comprehensive analysis and characterization of power loss of a high-power integrated gate-commutated thyristor (IGCT) in a modular multilevel converter (MMC) for a high voltage dc application. The practical scheme, power loss models, calculation methods, characterization of MMC based on IGCT are analyzed in detail. Especially, a comprehensive comparison of both half-bridge MMC (HB-MMC) and full-bridge MMC (FB-MMC) based on IGCT, press-pack insulated gate bipolar transistor (IGBT), module-type IGBT, press-pack injection enhanced gate transistor (IEGT), and module-type IEGT is analyzed in this paper. According to the study in this paper, the snubber power loss of MMC based on IGCT is far less than the conduction and switching power losses. Both the conduction and switching power losses of IGCT are always lower than that of press-pack and module-type IGBTs and IEGTs in MMC. The power loss of FB-MMC is higher than that of HB-MMC with the same transmission power because more switches are employed in FB-MMC. If taking diodes into account, the HB-MMC and FB-MMC based on IGCT can decrease power loss about 1.9%–49.3% and 8.3%–45.1% under different operation states, respectively. The study in this paper will provide a valuable reference and promote the application of IGCT in MMC.**

Index Terms—**High voltage dc (HVDC), injection enhanced gate transistor (IEGT), insulated gate bipolar transistor (IGBT), integrated gate-commutated thyristor (IGCT), modular multilevel converter (MMC), power loss.**

I. INTRODUCTION

HIGH voltage dc transmission technology based on voltage source converter (VSC-HVDC) can control active and reactive power independently and quickly, which enhances the flexibility of power transmission greatly and becomes one of the most potential technology for power transmission [1]–[5]. Recently, the VSC-HVDC technology is

developing rapidly; a lot of VSC-HVDC systems have been built all over the world and more systems are building [6]–[8].

In the VSC-HVDC system, the VSC is the most important core to achieve voltage conversion and power management. The solutions for VSC mainly contain two-level, three-level, and modular multilevel converters (MMCs) [9]–[11]. Compared with two-level and three-level converters, MMC employs a module-series technology and avoids switch series, which reduces the technical threshold of VSC-HVDC greatly. Moreover, MMC has advantages in power quality, power loss, reliability, and so on; therefore, MMC has become the hottest VSC technology for HVDC application, and most of the practical VSC-HVDC systems are built based on MMC after the finding of MMC [12]–[14].

Since insulated gate bipolar transistor (IGBT) has a lot of advantages, such as a simple driving circuit, low driving power, and fast switching speed, it has been widely used in the VSC-HVDC application [15], [16]. Especially, until now, almost all the commissioned MMC projects are built based on IGBT. Although IGBT has some outstanding advantages, compared with current-mode devices, the ON-state voltage drop of IGBT is still relatively high, and the current capability is still relatively low, so there is still plenty of room for improvement.

The applications of VSC-HVDC are now rapidly increasing, and the voltage and capacity of the VSC-HVDC system are becoming more demanding. In China, a dc transmission grid is under construction, and the voltage and capacity of the MMCs in which reaches ±500 kV/3000 MW. A ±800-kV/5000-MW MMC project is also under planning for long-distance bulk power transmission through overhead lines. In high-voltage and high-power MMC applications, there will be a strong attraction and great application prospect for the switching devices with higher current capability.

Because the number of levels of MMC is usually very high, a very low switching frequency can be used. Therefore, the conduction loss becomes prominent in the total loss of MMC, and the ON-state voltage drop of the switching devices become the chief factor of the efficiency. Half-bridge submodule-based MMCs (HB-MMCs) cannot block the dc-side short-circuit current, which limits its overhead line
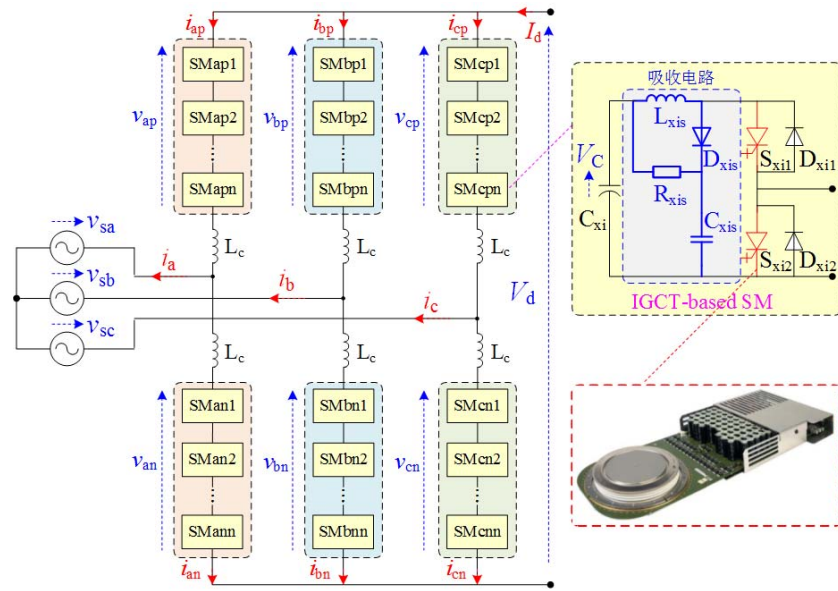
Fig. 1.   MMC based on IGCT.

applications. Some improved MMC topologies, such as full-bridge submodule-based MMCs (FB-MMCs), have dc fault blocking capability by employing additional switching devices in the submodule [17]. However, the arm current also flows through these additional switching devices and results in extra conduction losses. Switching devices with lower ON-state voltage drop become very attractive for these applications.

Compared with IGBT, the integrated gate-commutated thyristor (IGCT) has a lower ON-state voltage drop, especially the voltage and current capacities are higher, which may improve the performances of IGBT in high-voltage and high-power applications [18]–[20]. In fact, a key drawback for IGCT is slow switching speed, which cannot be accepted by most of VSC applications. However, in high-voltage and high-power MMC applications, the multilevel solution can improve the ac harmonic greatly, so the switching frequency of switches can be reduced significantly [21], [22], which weakens the drawback of IGCT and provides a good application opportunity.

However, until now, the application of IGCT in MMC is seldom discussed in the literature. References [23] and [24] discuss the potential of IGCT in HVDC application and the efficiency issue is also concerned; however, the analyses are still not detailed and comprehensive, especially some key conclusions about the power loss characterization of IGCT in the MMC application are not achieved. Based on the situation mentioned above, this paper gives a comprehensive analysis and characterization of IGCT in the MMC application. The study in this paper will provide a valuable reference and promote the application of IGCT in MMC.

This paper is organized as follows. Section II introduces the MMC-based IGCT and basic analytical models. Section III proposes power loss models for MMC based on IGCT, includes conduction loss, switching loo, and snubber loss models. Section IV gives power loss calculation demonstrations. On this basis, Section V gives a comprehensive power loss

characterization of MMC based on IGCT. Section VI compares the power loss performances of HB-MMCs based on IGCT, press-pack IGBT, module-type IGBT, press-pack injection enhanced gate transistor (IEGT), and module-type IEGT. Section VII further compares the power loss performances for FB-MMCs.

II. MMC BASED ON IGCT

A. Topology of MMC Based on IGCT

Fig. 1 shows the topology of MMC based on IGCT. The typical snubber circuit of IGCT is composed of a resistor R_{xis}, an inductor L_{xis}, a diode D_{xis}, and a capacitor C_{xis}. The inductor L_{xis} is employed to limit the current rise rate when IGCT is turned ON, the resistor R_{xis} is employed to absorb energy which stores in L_{xis} when IGCT is turned OFF. In addition, R_{xis}, C_{xis}, and D_{xis} also compose an RCD snubber circuit to limit overvoltage when IGCT is turned OFF [25]. In Fig. 1, x represents symbols ap, an, bp, bn, cp, or cn.

Beside the diffidence with MMC based on IGBT and IEGT, the issues about driving power source and retrigger should be designed carefully for MMC based on IGCT. In fact, the driving power source of the submodule in MMC based on IGCT should be shut down after the discharge of the dc capacitor of a submodule, or else the two IGCTs in submodule may turn ON because of a special mechanism of the IGCT driving circuit, which will cause a short-circuit fault. Thus, the driving power source should have high reliability and the power-OFF and power-ON logic should be designed carefully. Especially, because IGCT belongs to the current-controlled device, the driving power will be higher than that of IGBT and IEGT.

B. Basic Analytical Models of MMC

No matter IGCT based, IGBT based, or IEGT based, the operation of MMC is still similar; the basic operation
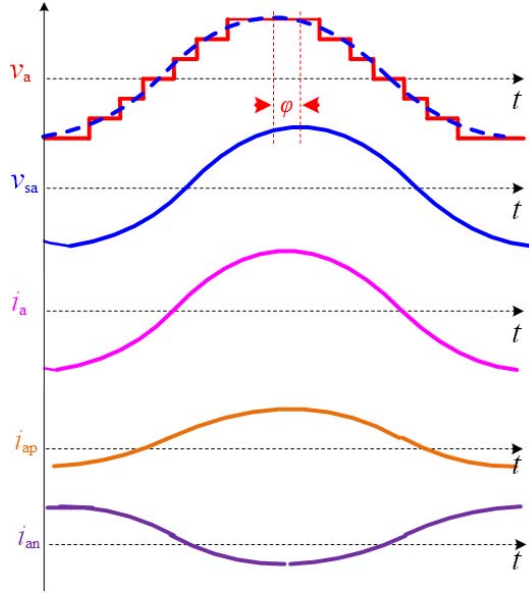
Fig. 2.   Basic operation waveforms of MMC.

waveforms of MMC are shown in Fig. 2. Each submodule generates a square wave with 50% duty ratio and there are different phase shifts between different submodules, so each arm will generate multilevel wave to imitate sine wave, we have

$$\begin{cases} v_{ap} = \dfrac{V_d}{2} - v_a \\ v_{an} = \dfrac{V_d}{2} + v_a \end{cases} \tag{1}$$

where v_{ap} and v_{an} are voltages of upper and lower arms in phase a, respectively, v_a is the equivalent output voltage of phase a, V_d is a dc voltage of MMC.

In a steady state, all the dc voltages of submodules are equal and can be defined V_C, we have

$$V_d = nV_C \tag{2}$$

v_a is generated by sine modulation, we have

$$v_a = M\frac{V_d}{2}\sin(wt) \tag{3}$$

where M is the modulation ratio and w is the angular frequency.

Then, the MMC can be equivalent to two sine voltages v_a and v_{sa} connected with an inductor, the magnitude and direction of power flow can be adjusted by controlling the magnitude and direction of phase shift angle φ between v_a and v_{sa}. The output ac current can be derived as

$$i_a(t) - i_a(0) = \int_0^t \frac{v_a - v_{sa}}{L}dt \tag{4}$$

where L is the equivalent inductance that contains arm inductance, transformer inductance, and ac grid inductance.

The arm currents can be derived as

$$\begin{cases} i_{ap} = \dfrac{i_a}{2} + \dfrac{I_d}{3} \\ i_{an} = -\dfrac{i_a}{2} + \dfrac{I_d}{3} \end{cases} \tag{5}$$
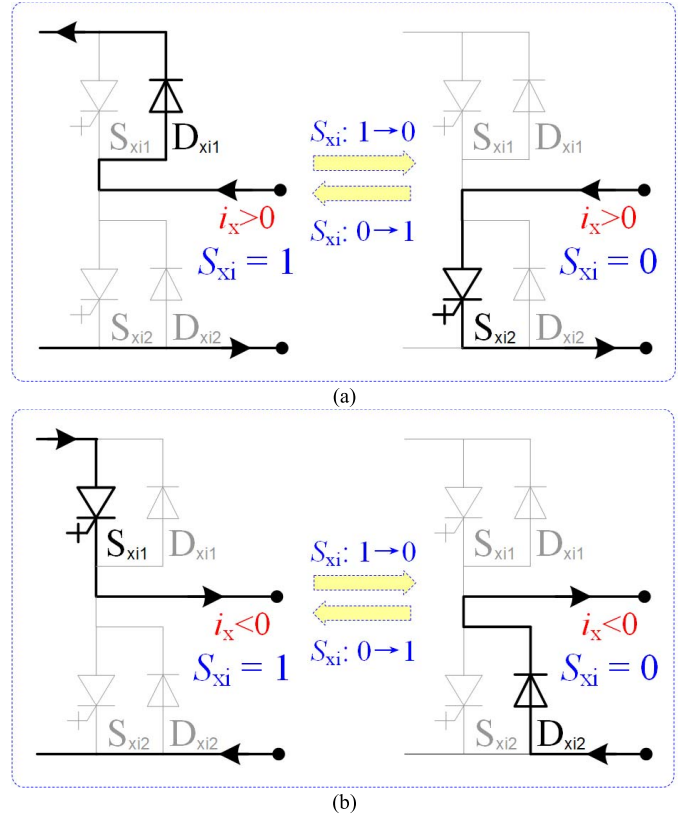
Fig. 3.   Commutation state of submodule in MMC based on IGCT. (a) $i_x > 0$. (b) $i_x > 0$.

where i_{ap} and i_{an} are currents of upper and lower arms in phase a, respectively, I_d is the dc current of MMC.

III. POWER LOSS MODEL OF MMC BASED ON IGCT

A. Conduction Loss Model for IGCT-MMC

Conduction power loss is mainly related to the current which flows through switches and diodes. For different operation states, the current flows through components will be different. However, if the arm current i_x (x represents ap, an, bp, bn, cp, or cn) and switching states of submodule are known, the current operation states will be known, as shown in Fig. 3. In Fig. 3, S_{xi} represents the switching function of the submodule. When S_{xi1} is turned ON and S_{xi2} is turned OFF, then $S_{xi} = 1$; when S_{xi1} is turned OFF and S_{xi2} is turned ON, then $S_{xi} = 0$.

The commutation behaviors of submodule in Fig. 3 can be summarized as Table I. When $i_x > 0$ and $S_{xi} = 1$, the current flows through the diode D_{xi1}; when $i_x > 0$ and $S_{xi} = 0$, the current flows through the switch S_{xi2}; when $i_x < 0$ and $S_{xi} = 1$, the current flows through the switch S_{xi1}; when $i_x < 0$ and $S_{xi} = 0$, the current flows through the diode D_{xi2}. Then, the current flows through the switches and diodes can be described as

$$\begin{cases} i_{Sxi1} = \text{ABS}[S_{xi}i_x\text{SGN}(-i_x)] \\ i_{Sxi2} = \text{ABS}[(1 - S_{xi})i_x\text{SGN}(i_x)] \\ i_{Dxi1} = \text{ABS}[S_{xi}i_x\text{SGN}(i_x)] \\ i_{Dxi2} = \text{ABS}[(1 - S_{xi})i_x\text{SGN}(-i_x)] \end{cases} \tag{6}$$

State	Bridge current	Switching function	Commutation behavior	Power loss
State 1	$i_{\text{brg}}>0$	$S_i=1$	D_{i1}	$v_{Di1}i_{Di1}$
State 2		$S_i=0$	S_{i2}	$v_{Si2}i_{Si2}$
State 3	$i_{\text{brg}}<0$	$S_i=1$	S_{i1}	$v_{Si1}i_{Si1}$
State 4		$S_i=0$	D_{i2}	$v_{Di2}i_{Di2}$
State 1→State 2		$S_i=1\to0$	$D_{i1}\downarrow\ S_{i2}\uparrow$	$E_{\text{Drec\_Di1}}, E_{\text{Son\_Si2}}$
State 2→State 1		$S_i=0\to1$	$D_{i1}\uparrow\ S_{i2}\downarrow$	$E_{\text{Soff\_Si2}}$
State 3→State 4		$S_i=1\to0$	$D_{i2}\uparrow\ S_{i1}\downarrow$	$E_{\text{Soff\_Si1}}$
State 4→State 3		$S_i=0\to1$	$D_{i2}\downarrow\ S_{i1}\uparrow$	$E_{\text{Drec\_Di2}}, E_{\text{Son\_Si1}}$

where $\text{SGN}(x)$ is a sign function, $\text{SGN}(x) = 1$ when $x > 0$, or else $\text{SGN}(x) = 0$; $\text{ABS}(x)$ is the absolute value function to get the positive value of current, i_{Sxi1}, i_{Sxi2}, i_{Dxi1}, and i_{Dxi2} are currents which flow through S_{xi1}, S_{xi2}, D_{xi1}, and D_{xi2}, respectively.

The transient conduction power loss can be derived based on the product of current and voltage drop of switches and diodes. The datasheet of switches and diodes usually provide the relationship curve between the voltage drop and the conducting current. The typical mathematical method is to linearize the relationship curve with two sections, then the voltage drop of switches and diodes in the submodule can be derived as

$$\begin{cases} v_{Sxi1} = V_{S0} + R_S i_{Sxi1} \\ v_{Sxi2} = V_{S0} + R_S i_{Sxi2} \\ v_{Dxi1} = V_{D0} + R_D i_{Dxi1} \\ v_{Dxi2} = V_{D0} + R_D i_{Dxi2} \end{cases} \quad (7)$$

where v_{Sxi1}, v_{Sxi2}, v_{Dxi1}, and v_{Dxi2} are voltage drops of S_{xi1}, S_{xi2}, D_{xi1}, and D_{xi2}, respectively, V_{S0} and V_{D0} are the threshold voltage of switch and diode, respectively, R_S and R_D are slope resistance.

Then, the conduction power loss of a submodule in MMC can be derived as

$$P_{\text{cond\_}xi} = \frac{1}{T}\int_0^T \left(v_{Sxi1}i_{Sxi1} + v_{Sxi2}i_{Sxi2} \right.$$
$$\left. + v_{Dxi1}i_{Dxi1} + v_{Dxi2}i_{Dxi2}\right)dt \quad (8)$$

where T is a line frequency.

Therefore, the conduction power loss of a whole MMC can be achieved by adding the conduction power losses of all the submodules.

B. Switching Loss Model for IGCT-MMC

Since the turn-ON and turn-OFF processes of switches and diodes are not ideal, the voltage is increasing (or decreasing) while the current is decreasing (or increasing) in the switching process, then the switching power loss is caused and it can be calculated by multiplying the voltage and current in the switching process. For different operation states of MMC, the switching behaviors of switches and diodes are different, as shown in Fig. 3.

When $i_x > 0$ and S_{xi}: $1 \to 0$, the diode D_{xi1} turns OFF, and the switch S_{xi2} turns ON, the switching power losses contain:

turn-OFF loss of D_{xi1} and turn-ON loss of S_{xi2}. When $i_x > 0$ and S_{xi}: $0 \to 1$, the diode D_{xi1} turns ON, and the switch S_{xi2} turns OFF, because the turn-ON loss of the diode is very small and it is usually can be ignored, so the switching power loss just contain turn-OFF loss of S_{xi2}. When $i_x < 0$ and S_{xi}: $1 \to 0$, the diode D_{xi2} turns ON, the switch S_{xi1} turns OFF, the switching power losses contain: turn-OFF loss of S_{xi1} and turn-ON loss of D_{xi2}. When $i_x < 0$ and S_{xi}: $0 \to 1$, the diode D_{xi2} turns OFF, the switch S_{xi1} turns ON, the switching power losses contain: turn-OFF loss of D_{xi2} and turn-ON loss of S_{xi1}.

For IGBT and IGCT, the datasheet of switches and diodes usually provides the turn-ON and turn-OFF energies ($E_{\text{Son\_N}}$ and $E_{\text{Soff\_N}}$) at certain voltage and current conditions. For a diode, the datasheet usually provides the reverse recovery energy at certain voltage and current conditions. In practice, the switching energy can be calculated based on the voltage and current at switching time, we have

$$\begin{cases} E_{\text{Son}} = \dfrac{V_C I_{\text{Son}}}{V_{S\_N} I_{S\_N}} E_{\text{Son\_N}} \\[2mm] E_{\text{Soff}} = \dfrac{V_C I_{\text{Soff}}}{V_{S\_N} I_{S\_N}} E_{\text{Soff\_N}} \\[2mm] E_{\text{Drec}} = \dfrac{V_C I_{\text{Drec}}}{V_{D\_N} I_{D\_N}} E_{\text{Drec\_N}} \end{cases} \quad (9)$$

where V_{S_N}, I_{S_N} and V_{D_N}, I_{D_N} are certain voltage and current of switches and diodes in the datasheet, E_{Son}, E_{Soff}, and E_{Drec} are switching energies in practice, I_{Son}, I_{Soff}, and I_{Drec} are currents at switching time and they are changing with the change of the operation state of a submodule.

Adding the switching energy when a switching behavior occurs, then the switching power loss of a submodule in MMC can be achieved by adding all the switching energies in 1 s. Therefore, the switching power loss of a whole MMC can be achieved by adding the switching power losses of all the submodules.

C. Snubber Loss Model for IGCT-MMC

Compared with MMC based on IGBT and IEGT, there is a *di/dt* snubber circuit in MMC based on IGCT, so additional snubber power loss should be considered. From Fig. 3, when $i_x < 0$ and S_{xi} is switched from 0 to 1, the inductor L_{xis} will store energy; when S_{xi} is switched from 1 to 0, the energy in inductor L_{xis} will release energy. Fig. 4 shows possible paths for inductor L_{xis} to release energy. From Fig. 4, the stored energy not only dissipates in the RCD snubber circuit but also provides the turn-OFF loss of IGCT; moreover, a small part energy flows to the dc capacitor C_{xi}. However, according to the analysis in [26], 80%–90% stored energy of L_{xis} in the turn-ON process will dissipate in a snubber circuit.

Similarly, the situation is the same when $i_x > 0$. Therefore, the snubber energy loss of a submodule of MMC based on IGCT in a switching period can be calculated approximately

$$E_{\text{Snubber}} = \frac{1}{2}L_{xis}I_{\text{snubber}}^2 \quad (10)$$

where I_{snubber} is the arm current when S_{xi} is switched between 0 and 1.
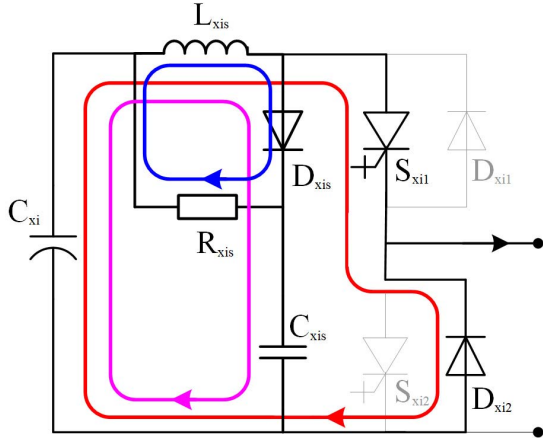
Fig. 4. Possible paths for inductor L_{xis} to release energy.

Then, the switching power loss of snubber in a submodule can be achieved by adding all the snubber energy in 1 s. Therefore, the snubber power loss of a whole MMC based on IGCT can be achieved by adding the snubber power losses of all the submodules.

IV. POWER LOSS SIMULATION CALCULATION OF MMC BASED ON IGCT

According to the analysis in Section III, the power losses of MMC based on IGCT are related with device current, voltage, and switching behaviors, which is very complicate to calculate. In this paper, the power loss model of IGCT and the commutation characteristics of MMC are combined, the power loss of MMC can be obtained by employing MATLAB. The calculation method in this paper is simple and effective, which can be used with different MMC topologies easily.

A. Conduction Loss for IGCT-MMC

Fig. 5 shows a calculation demonstration of conduction power loss for MMC based on IGCT. First, according to the analysis in Section II, the arm current and switching signals can be obtained based on the specified operation state and modulation method. Then, from (6) and (7), the conducting current and voltage drop of all the switches and diodes can be obtained. The transient power loss can be achieved by multiplying current and voltage, then the conduction loss energy during one operation period can be obtained based on the integral of transient power loss, which is indicated by the shaded area in Fig. 5. Then, the conduction power loss of a submodule can be obtained by adding the conduction loss energy during 1 s. In Fig. 5, the parameters of MMC are the same as Section V, and the MMC operates in the rectifier state with −600-MW transmission power.

B. Switching Loss for IGCT-MMC

Fig. 6 shows a calculation demonstration of switching power loss for MMC based on IGCT. First, according to the analysis in Section II, the arm current and switching signals can be obtained based on the specified operation state
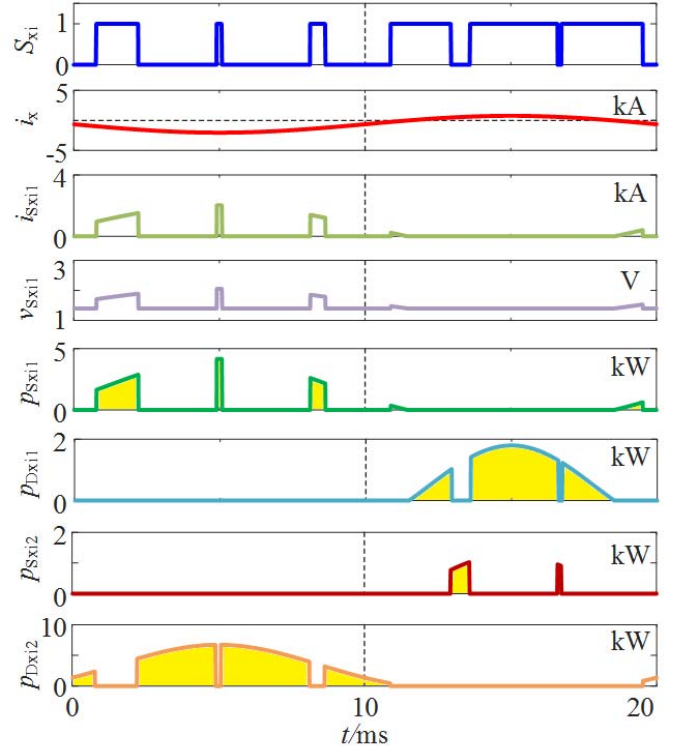

Fig. 5. Calculation demonstration of conduction power loss for MMC based on IGCT.
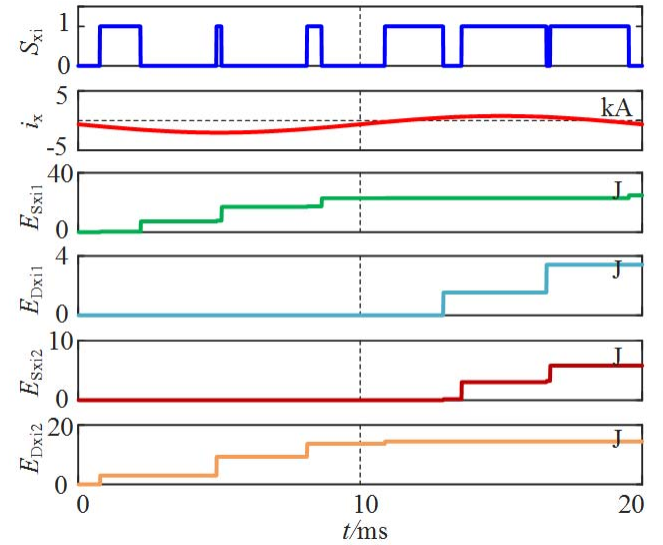

Fig. 6. Calculation demonstration of switching power loss for MMC based on IGCT.

and modulation method. From Section IV-A, the switching behaviors and related energy losses can be derived based on the switching states and current polarity at switching time. Then, accumulating the energy losses at every switching time one by one, the switching losses of all the switches and diodes can be obtained. Therefore, the switching losses of a submodule can be obtained by adding the switching losses of all the switches and diodes during 1 s.
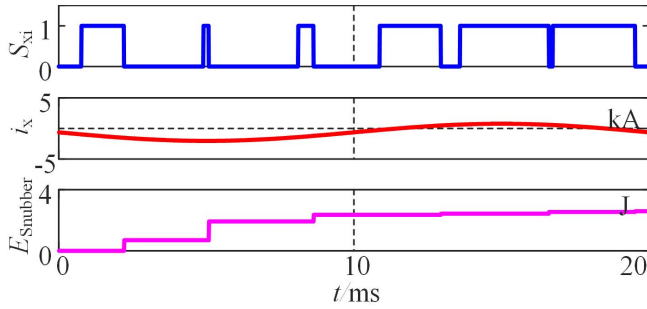
Fig. 7. Calculation demonstration of snubber power loss for MMC based on IGCT.

TABLE II
PARAMETERS OF MMC BASED ON IGCT FOR
POWER LOSS CHARACTERIZATION

Parameter	Unit	Value
Power	MVA	600
AC grid voltage	kV	110
AC terminal voltage of MMC	kV	175
DC terminal voltage of MMC	kV	320
Turn ratio of transformer	1	0.629
DC voltage of sub-module	V	2200
Number of sub-module	1	145
DC capacitance of sub-module	μF	15117
Inductance of AC grid	mH	18.27
Inductance of transformer	mH	19.50
Inductance of MMC arm	mH	32.49
Capacitance of snubber	μF	3.8
Inductance of snubber	μH	0.6
Resistance of snubber	Ω	0.76
IGCT model	- -	5SHY 35L4521
Diode model	- -	5SDF 20L4520

C. Snubber Loss Calculation for IGCT-MMC

The calculation of snubber power loss is similar to the switching power loss. Fig. 7 shows a calculation demonstration of snubber power loss for MMC based on IGCT. First, according to the analysis in Section II, the arm current and switching signals can be obtained based on the specified operation state and modulation method. From Section V-A, there will be a snubber energy loss for every turn OFF of IGCT. Therefore, we just need to accumulate the energy losses at every period one by one, then the snubber loss of a submodule can be obtained by adding the snubber losses during 1 s.

V. POWER LOSS CHARACTERIZATION OF MMC BASED ON IGCT

A. Analytical Parameters Based on Practical HVDC Project

In order to analyze the power loss characterization of MMC based on IGCT, the Nanao project (the first multiterminal VSC-HVDC system in the world) is taken as a target. The IGCT is 5SHY 35L4521 produced by ABB. The design parameters are shown in Table II.

B. Power Loss Distribution for IGCT-MMC

Based on the above-mentioned analysis, Fig. 8 shows the different components of power loss for MMC based on IGCT under rectifier, inverter, and reactive power states.

For conduction power loss, the power is transferred from ac to dc side under rectifier state, the arm current i_x has a negative bias, and the current flows through the upper switch and lower diode during most of the time. From Fig. 5, $S_{xi} = 0$ for most of the time when $i_x < 0$, so the current flows through D_{xi2} during most of the time, and the conduction power loss of D_{xi2} is the highest. Similarly, in the inverter state, the power is transferred from dc to ac side, the arm current i_x has a positive bias, and the current flows through S_{xi2} and D_{xi1} during most of the time. $S_{xi} = 0$ for most of the time when $i_x > 0$, so the current flows through S_{xi2} during most of the time, and the conduction power loss of S_{xi2} is the most. In reactive power, the active power is zero, the arm current i_x has no bias, and the current flows through S_{xi2}/D_{xi1} and S_{xi1}/D_{xi2} with similar time, so the conduction power losses of components are similar.

For switching power loss, because the transmission power under rectifier and inverter states are the same, just the direction of power flow is opposite, so the switching power losses of the upper switch under rectifier and inverter states are basically the same with that of the lower switch under inverter and rectifier states, respectively. In reactive power state, the upper and lower switches have the same switching power losses. The same features are also for upper and lower diodes.

For snubber power loss, it has a little difference under different operation states with the same power. The snubber power loss in the rectifier state is higher than that in inverter and reactive power states, and the reactive power state has the lowest snubber power loss. However, no matter any operation state, the snubber power loss of MMC based on IGCT is far less than the conduction and switching power losses.

C. Power Loss of IGCT-MMC with Different Frequencies

Fig. 9 shows the power loss of MMC based on IGCT with different switching frequencies. It can be seen that the switching power losses of IGCT and diode and the snubber power loss increase with the increase in the switching frequency under rectifier, inverter, and reactive power states. The power loss under reactive power state is lower than that under an active power state, and the rectifier state has the highest power loss. With the low switching frequency, the conduction power loss is higher than the switching power loss. However, as the increase in the switching frequency, the switching power loss will become higher. The snubber power loss is always far less than the conduction and switching power losses.

D. Power Loss of IGCT-MMC with Different Powers

Fig. 10 shows the power loss of MMC based on IGCT with different powers. It can be seen that the power losses of IGCT and diode and the snubber power loss increase with the increase in power under rectifier, inverter, and reactive power states. Under the rectifier state, the power is transferred from ac to dc side, so the negative part of bridge-arm currents is more than the positive part, the current flows as Fig. 3(b) in most of the time, then the switch S_{i1} and the diode D_{i2} take most of the loss. Under the inverter state, the power
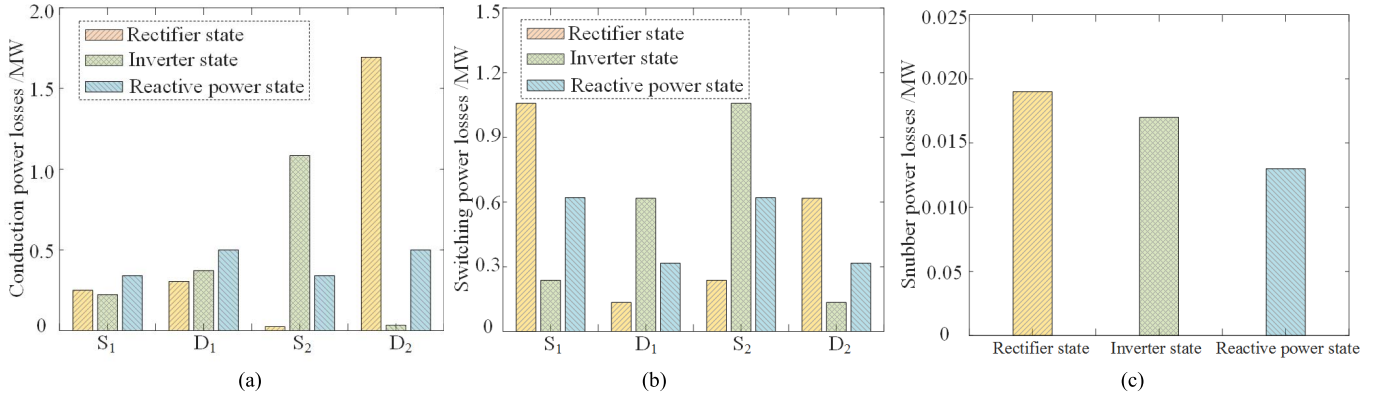
Fig. 8. Different components of power loss for MMC based on IGCT. (a) Conduction power loss. (b) Switching power loss. (c) Snubber power loss.
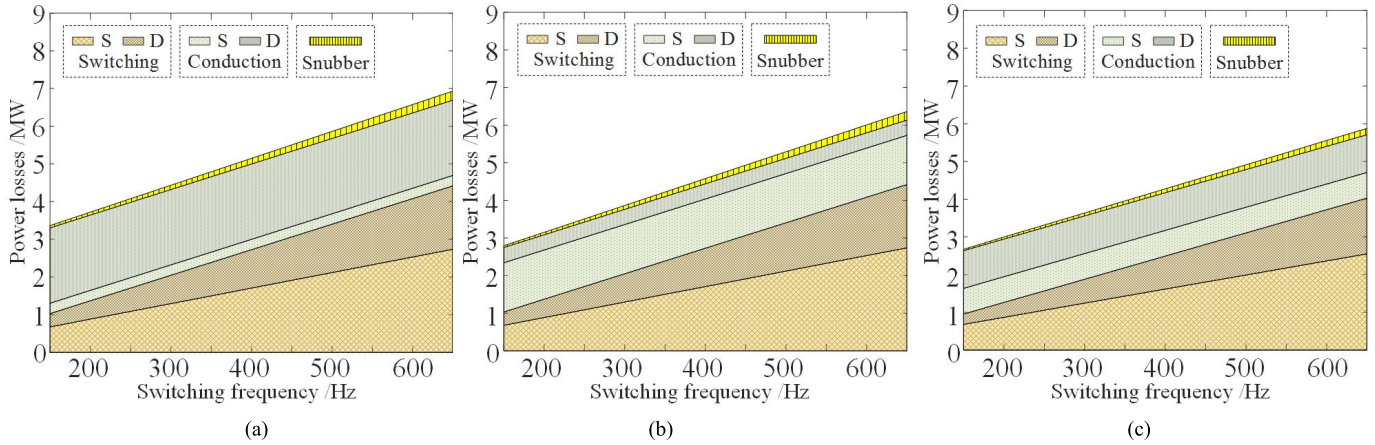

Fig. 9. Power loss of MMC based on IGCT with different switching frequencies. (a) Rectifier state. (b) Inverter state. (c) Reactive power state.
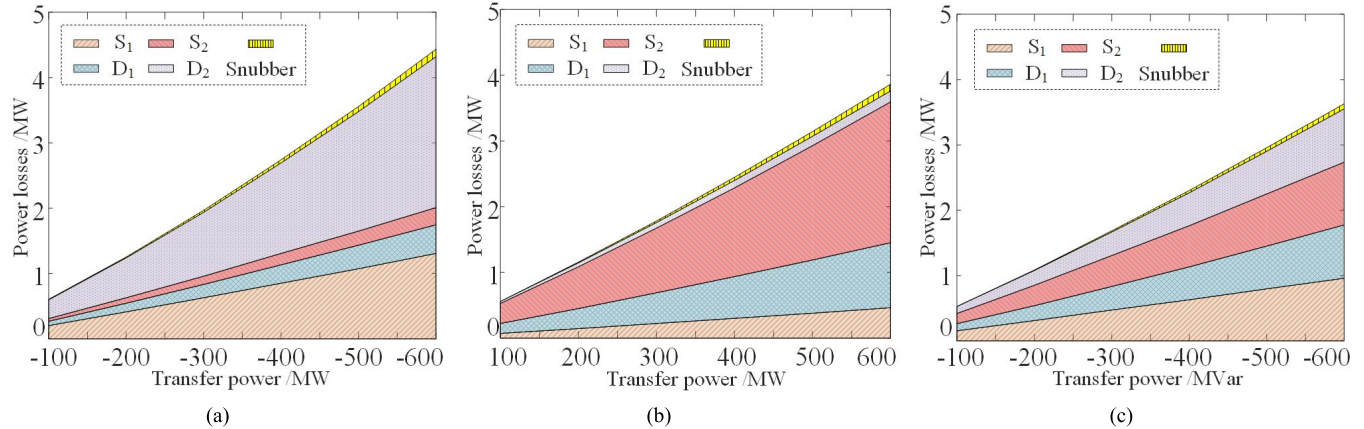

Fig. 10. Power loss of MMC based on IGCT with different powers. (a) Rectifier state. (b) Inverter state. (c) Reactive power state.

is transferred from dc to ac side, so the positive part of bridge-arm currents is more than the negative part, the current flows as Fig. 3(a) in most of the time, then the switch S_{i2} and the diode D_{i1} take most of the loss. Under the reactive power state, there is no power transmission in the dc side, so the positive part of bridge-arm currents is almost the same with the negative part, and then the upper and lower devices almost take the same power losses.

In Figs. 8–10, the transmission powers are −600 MW, 600 MW, and 600 MVar for rectifier, inverter, and reactive power states, respectively. The power losses of S_1, D_1, S_2,

and D_2 are the sum of all the components in the same position (upper IGCT, upper diode, lower IGCT, and lower diode) of submodules.

VI. Power Loss Comparison of MMCs Based on IGCTs, IGBTs, and IEGTs

At present, almost all the MMCs in the world are built based on IGBT, and few MMCs are built based on IEGT; this paper will give a comprehensive comparison about power loss for MMCs based on IGCT, IGBT, and IEGT.
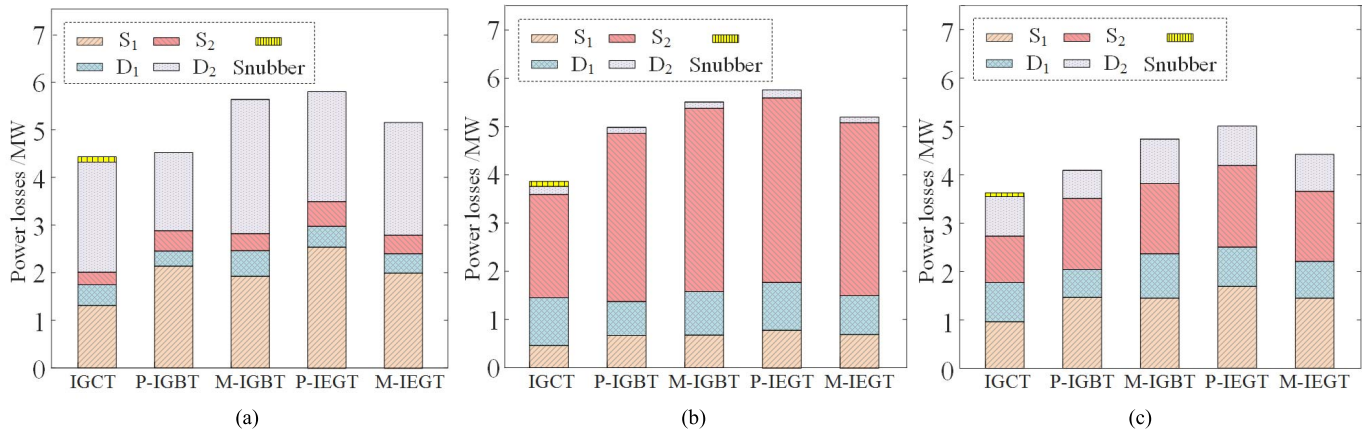
Fig. 11. Power loss comparison with different components for MMCs based on IGCTs, IGBTs, and IEGTs. (a) Rectifier state. (b) Inverter state. (c) Reactive power state.

A. IGCT, IGBT, and IEGT for Comparison

For MMCs based on IGCT, IGBT, and IEGT with the same voltage, the characteristic operation currents and voltages are almost the same, the power loss is different because the performance of IGCT, IGBT, and IEGT are different, and the snubber circuit is added for MMC based on IGCT. In order to compare the power loss of MMCs based on IGCT, IGBT, and IEGT for HV MW applications, the 4.5-kV IGCT, press-pack IGBT, module-type IGBT, press-pack IEGT, and module-type IEGT produced by ABB and TOSHIBA are employed, and all the devices are commercial products, as shown in Fig. 3. In fact, the definition of current rating for IGCT in practice is different with IGBT and IEGT, the maximum turn-OFF current is a current rating for IGCT and the dc collector current is a current rating for IGBT or IEGT. In this paper, the 4500-V/4000-A IGCT is employed for the IGCT analysis, the average ON-state current is 1700 A, and the current rating is the closest during all the commercialized IGCTs to the current rating 2000 A of the employed press-pack IGBT and IEGT. As for module-type devices, the current rating is smaller than that of press-pack devices, we choose the maximum current rating of 1200 A in commercialized module-type IGBT and IEGT produced by ABB to analyze.

B. Comparison of Power Loss Distribution

Fig. 11 shows power losses distribution for different components in MMC based on IGCTs, IGBTs, and IEGTs. Similar with the analysis in Section V, no matter IGCT, IGBT, or IEGT-based MMC, the switch S_{i1} and the diode D_{i2} take most of the loss under the rectifier state, the switch S_{i2} and the diode D_{i1} take most of the loss under the inverter state, and the upper and lower devices almost take the same power loss under reactive power state. From Fig. 11, the MMC based on IGCT has the lowest power loss and the MMC based on press-pack IEGT has the highest power loss. Moreover, if we just consider switches, both the upper and lower IGCT switches S_1 and S_2 also have the lowest power losses during all the operation states of MMC.

Fig. 12 shows the power loss distribution for different types in MMC based on IGCTs, IGBTs, and IEGTs. No matter what operation states for MMC, the MMC based on IGCT always has the lowest switching loss, and the MMC based on press-pack IEGT has the highest switching loss. As for conduction loss, the MMC based on IGCT has the lowest power loss during inverter and reactive power states, but the MMC based on press-pack IGBT has the lowest conduction loss during the rectifier state because the press-pack IGBT has lower diode conduction loss. However, if we just consider switches, both the conduction and switching power losses of IGCT are always lower than that of IGBTs and IEGTs. This finding is different from the common sense that IGCT just has lower conduction power loss but the switching power loss is higher. In fact, from Table III, although the turn-OFF energy of IGCT is higher than that of IGBTs and IEGTs with the same voltage and current conditions, the turn-ON energy of IGCT is far lower than that of IGBTs; therefore, the switching power loss of IGCT is possible to be lower.

Similar with the operation of MMC in Section V, the transmission powers of −600 MW, 600 MW, and 600 MVar for rectifier, inverter, and reactive power states are shown in Figs. 11–13. Table IV summarizes the power loss results of MMC based on IGCTs, IGBTs, and IEGTs during the rated operation. Under the rectifier state, compared with the MMC based on IGCT, the MMCs based on press-pack IGBT, module-type IGBT, press-pack IEGT, and module-type IEGT increase the loss by 1.9%, 26.9%, 31.2%, and 16.6%, respectively. Under the inverter state, the MMCs based on press-pack IGBT, module-type IGBT, press-pack IEGT, and module-type IEGT increase the loss by 28.8%, 42.4%, 49.3%, and 34.8%, respectively. Under the reactive power state, the MMCs based on press-pack IGBT, module-type IGBT, press-pack IEGT, and module-type IEGT increase the loss by 12.7%, 30.3%, 38.0%, and 21.7%, respectively.

C. Comparison of Power Loss with Different Switching Frequencies

Fig. 13 shows the power loss of MMC with different switching frequencies. It can be seen that no matter IGCTs,
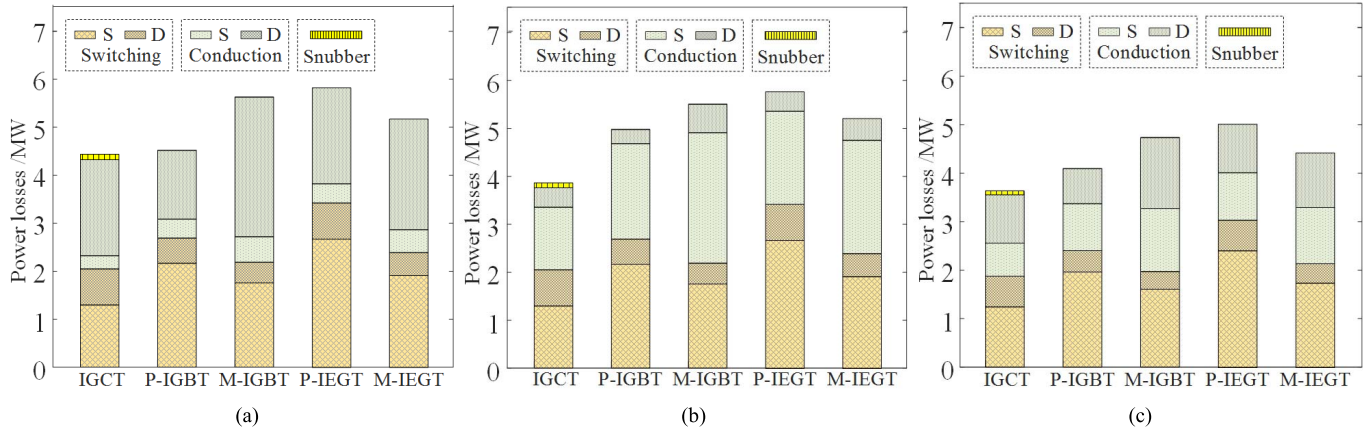
Fig. 12. Power loss comparison with different types for MMCs based on IGCTs, IGBTs, and IEGTs. (a) Rectifier state. (b) Inverter state. (c) Reactive power state.

TABLE III
PARAMETERS OF IGCTs, IGBTs, AND IEGTs FOR COMPARISON

Device	IGCT	Press-pack IGBT		Module-type IGBT		Press-pack IEGT	Module-type IEGT		Press-pack Diode
Manufacturer	ABB	ABB		ABB		TOSHIBA	TOSHIBA		ABB
Model	5SHY 35L4521	5SNA 2000K450300		5SNA 1200G450300		ST2100GXH24A	MG1200GXH1US61		5SDF 20L4520
Blocking voltage	4500 V	4500 V		4500 V		4500 V	4500 V		4500 V
Max. turn-off current I_{TGQM}	4000 A	—		—		—	—		—
Average on-state current $I_{T/F(AV)M}$	1700 A	—		—		—	—		1950 A
DC/Peak collector current I_C/I_{CM}	—	2000 A/4000 A		1200 A/2400 A		2100 A/4200 A	1200 A/2400 A		—
Part	GCT-part	IGBT-part	Diode-part	IGBT-part	Diode-part	IEGT-part	IEGT-part	Diode-part	Diode-part
Threshold voltage V_{S0}/V_{D0} (125℃)	1.4 V	1.4 V	1.3 V	1.6 V	2.6 V	1.73 V	1.84 V	1.6 V	1.7 V
Slope resisance R_S/R_D(125℃)	0.325 mΩ	1.0 mΩ	0.52 mΩ	1.58 mΩ	1.08 mΩ	0.72 mΩ	1.06 mΩ	1.17 mΩ	0.8 mΩ
Turn-on energy E_{on} (125℃)	1.5 J	11 J	—	4.35 J	—	15 J	5.7 J	—	—
Turn-off energy E_{off}/E_{rec}(125℃)	22 J	10.5 J	5.5 J	6.0 J	2.73 J	12 J	5.7 J	3.0 J	13 J
Meas. condition	2800 V/4000 A	2800 V/2000 A		2800 V/1200 A		2700 V/2100 A	2800 V/1200 A		2800 V/3300 A
Max Junction operating temperature T_{vj}	125℃	125℃	125℃	125℃	125℃	125℃	150℃	150℃	140℃

TABLE IV
POWER LOSS RESULTS OF MMC BASED ON IGCTs, IGBTs, AND IEGTs

Type	P_{loss}/kW	P_{CON}/kW	P_{SW}/kW	P_{Snu}/kW	P_{CON} (S) /kW	P_{SW} (S) /kW
Rectifier state with *P* = -600 MW						
IGCT	4437	2274	2049	114	275	1296
Press IGBT	4521	1831	2690	0	395	2166
Module IGBT	5631	3442	2189	0	529	1756
Press IEGT	5820	2396	3424	0	397	2674
Module IEGT	5172	2779	2393	0	474	1917
Inverter state with *P* = 600 MW						
IGCT	3865	1714	2049	102	1308	1296
Press IGBT	4977	2287	2690	0	1992	2166
Module IGBT	5505	3316	2189	0	2720	1755
Press IEGT	5770	2345	3425	0	1939	2674
Module IEGT	5210	2817	2393	0	2361	1917
Reactive power state with *Q* = -600 MVar						
IGCT	3636	1681	1877	78	681	1243
Press IGBT	4098	1694	2403	0	969	1962
Module IGBT	4736	2761	1975	0	1293	1610
Press IEGT	5017	1977	3039	0	977	2407
Module IEGT	4424	2284	2140	0	1165	1739

on IGCT always has the lowest power loss under inverter and reactive power states. Under the rectifier state, the MMC based on press-pack IGBT has the lowest power loss when the frequency is low. However, this is because the power loss of diodes integrated into press-pack IGBT is lower in this area, and the power loss caused by IGCT is still lower than that caused by press-pack IGBT.

D. Comparison of Power Loss with Different Powers

Fig. 14 shows the power loss of MMC with different powers. It can be seen that the MMC based on IGCT always has the lowest power loss during rectifier, inverter, and reactive power states, and the MMC based on press-pack IEGT has the highest power loss. In Fig. 14, because of the limitation of the modulation ratio of MMC, the maximum reactive power that can generate to power grid for MMC is just about 200 MVar.

VII. POWER LOSS COMPARISON OF FB-MMCs BASED ON IGCTs, IGBTs, AND IEGTs

In the above-mentioned analysis, the MMC is mainly based on HB-MMC. However, HB-MMC cannot block the dc-side short-circuit current, which limits its overhead line applications. The MMC based on FB-MMC is currently a popular

IGBTs, and IEGTs based, the power loss of MMC increases with the increase in the switching frequency. The MMCs based on module-type IGBT and press-pack IEGT have the highest power loss during all the range. The MMC based
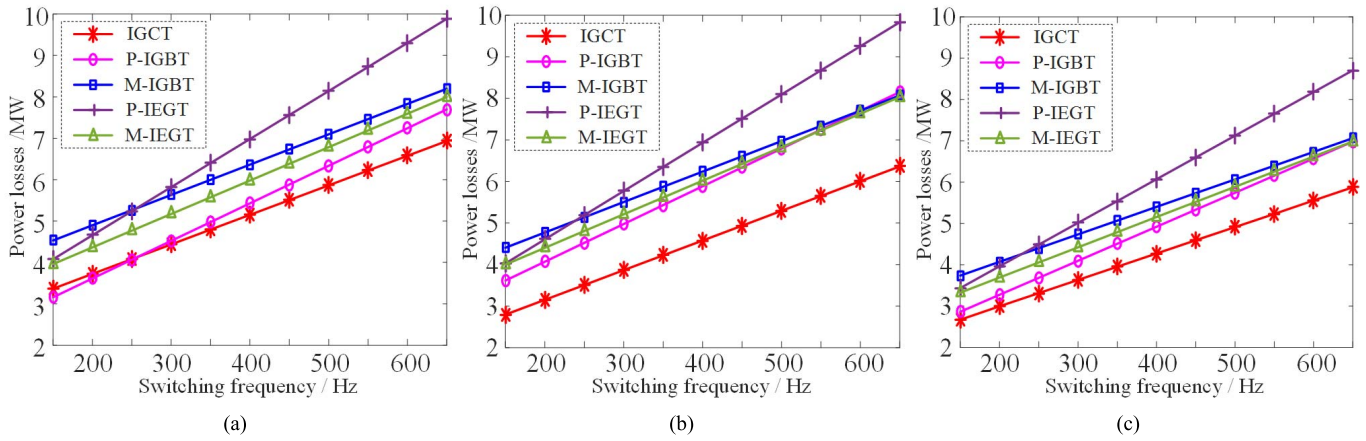
Fig. 13. Power loss with different switching frequencies for MMCs based on IGCTs, IGBTs, and IEGTs. (a) Rectifier state. (b) Inverter state. (c) Reactive power state.
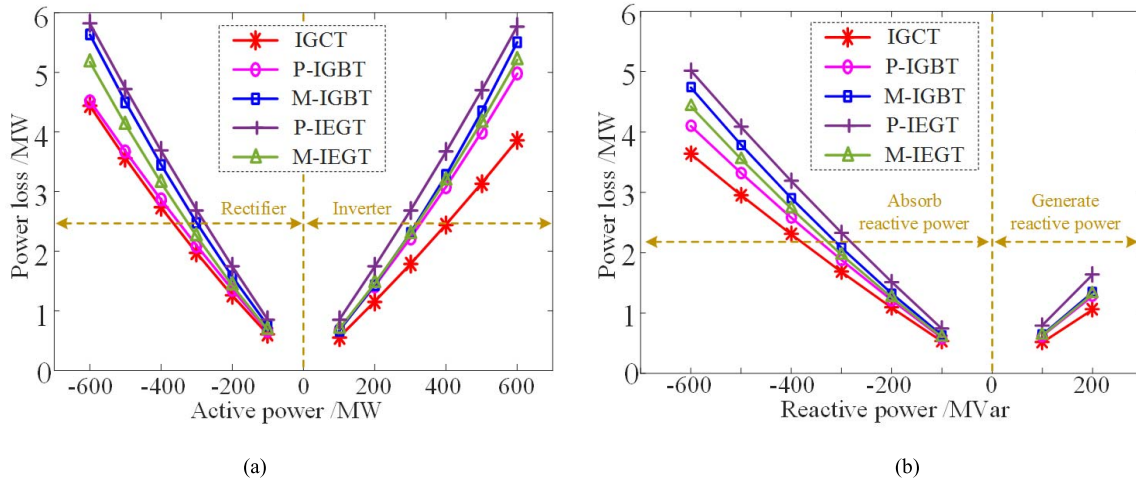

Fig. 14. Power loss with different powers for MMCs based on IGCTs, IGBTs, and IEGTs. (a) Active power transfer. (b) Reactive power transfer.
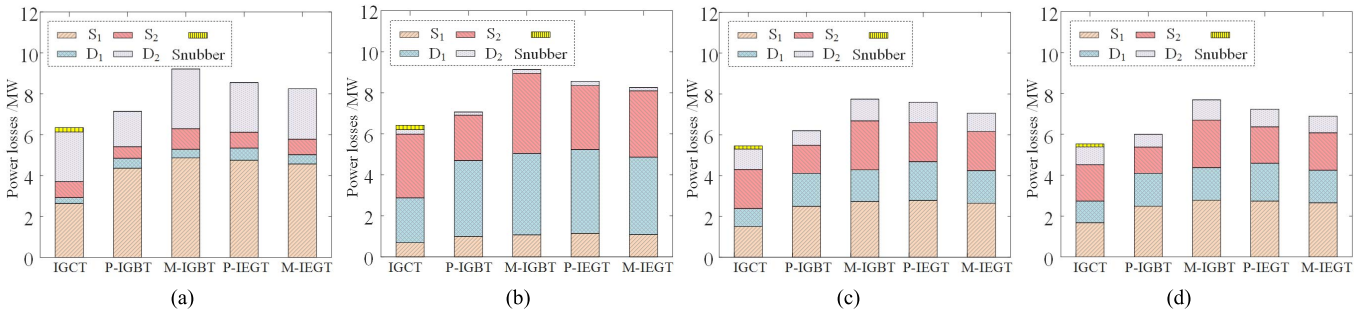

Fig. 15. Power loss comparison with different components for FB-MMCs based on IGCTs, IGBTs, and IEGTs. (a) Rectifier state. (b) Inverter state. (c) Absorb reactive power state. (d) Generate reactive power state.

scheme to block dc-side short-circuit fault by employing additional switching devices in the submodule. This section will give a power loss comparison about FB-MMC.

A. Comparison of Power Loss Distribution

Fig. 15 shows a power loss distribution for different components in FB-MMCs based on IGCTs, IGBTs, and IEGTs. Similar to the analysis in Section VI, the upper switches and the lower diodes take most of the loss under rectifier state, the lower switches and the upper diodes take most of the loss under inverter state, and the power loss difference is not significant under reactive power states. The FB-MMC based on IGCT still has the lowest power loss; however, the power loss for FB-MMC based on module-type IGBT changes to be the highest.

In fact, as shown in Fig. 16, compared with HB-MMC, the conduction power loss changes to be greater for FB-MMC.
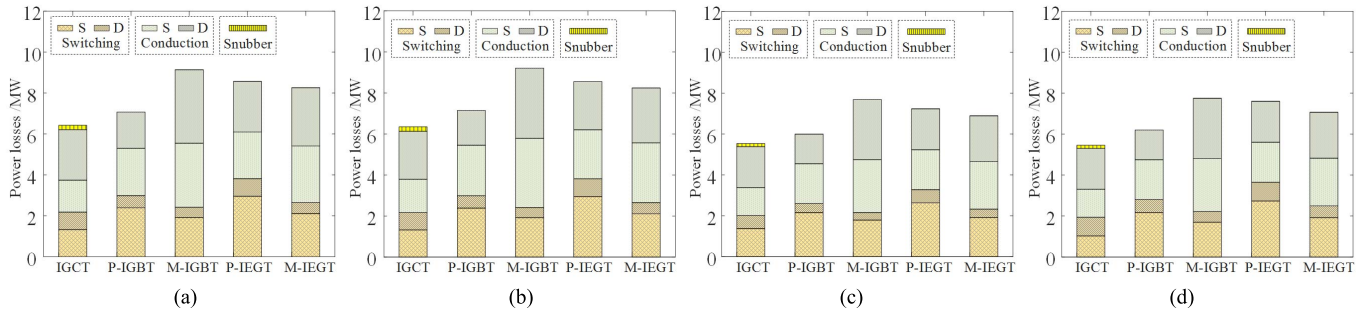
Fig. 16. Power loss comparison with different types for FB-MMCs based on IGCTs, IGBTs, and IEGTs. (a) Rectifier state. (b) Inverter state. (c) Absorb reactive power state. (d) Generate reactive power state.
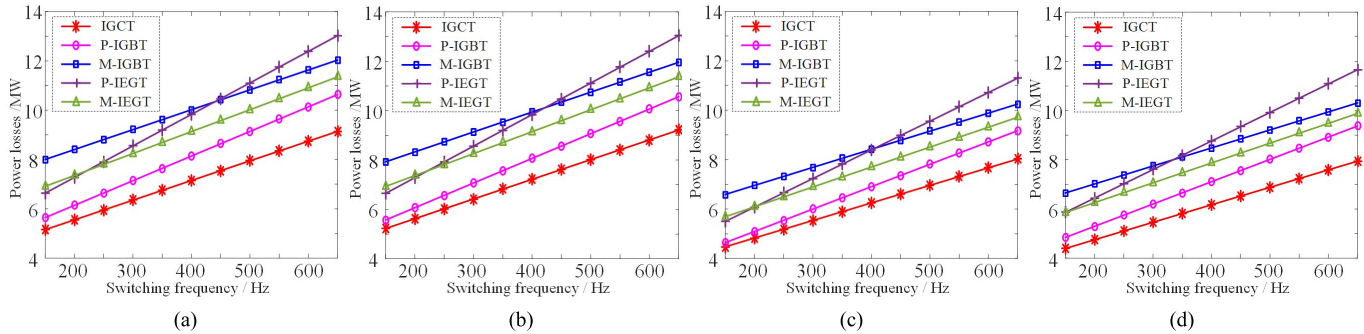

Fig. 17. Power loss comparison with switching frequency for FB-MMCs based on IGCTs, IGBTs, and IEGTs. (a) Rectifier state. (b) Inverter state. (c) Absorb reactive power state. (d) Generate reactive power state.
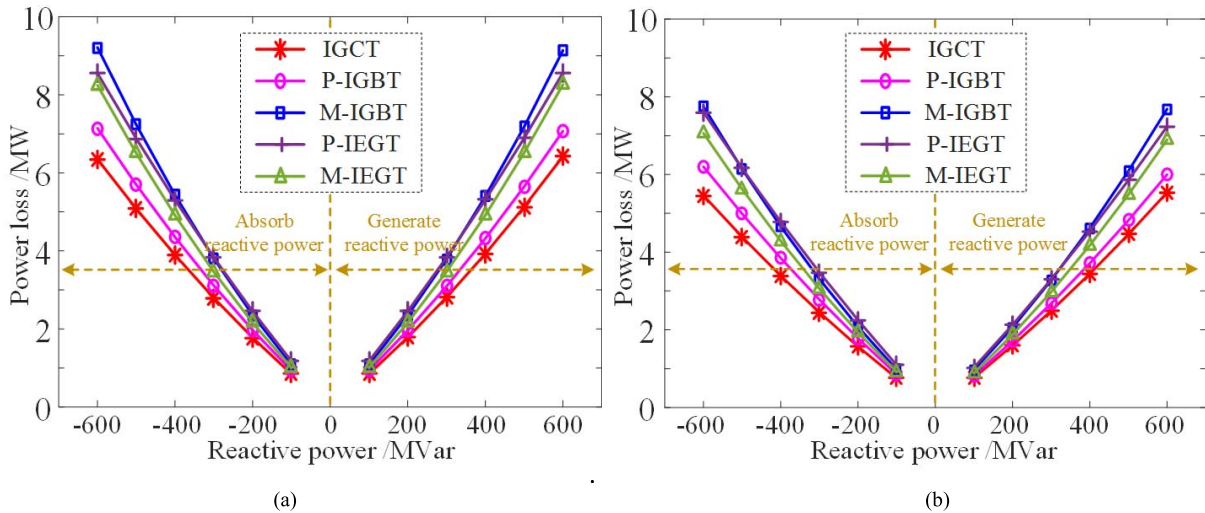

Fig. 18. Power loss with different powers for FB-MMCs based on IGCTs, IGBTs, and IEGTs. (a) Active power transfer. (b) Reactive power transfer.

Because the conduction performance of press-pack IEGT is better than that of module-type IGBT, so the FB-MMC based on module-type IGBT has the highest power loss. No matter any case, if we just consider switches, both the conduction and switching power losses of IGCT are always lower than that of IGBTs and IEGTs. This finding is the same as HB-MMC.

Table V summarizes the power loss results of FB-MMC based on IGCTs, IGBTs, and IEGTs during the rated operation. Under rectifier state, compared with the FB-MMC based on IGCT, the FB-MMCs based on press-pack IGBT,

module-type IGBT, press-pack IEGT, and module-type IEGT increase the loss by 10.1%, 42.3%, 33.3%, and 28.6%, respectively. Under the inverter state, the FB-MMCs based on press-pack IGBT, module-type IGBT, press-pack IEGT, and module-type IEGT increase the loss by 12.5%, 45.1%, 34.7%, and 29.8%, respectively. Under the reactive power state with $Q = -600$ MVar, the FB-MMCs based on press-pack IGBT, module-type IGBT, press-pack IEGT, and module-type IEGT increase the loss by 8.3%, 38.8%, 30.7%, and 24.5%, respectively. Under the reactive power state with $Q = 600$ MVar,

TABLE V
POWER LOSS RESULTS OF FB-MMC BASED
ON IGCTs, IGBTs, AND IEGTs

Type	P_{loss}/kW	P_{CON}/kW	P_{SW}/kW	P_{Snu}/kW	P_{CON} (S) /kW	P_{SW} (S) /kW
Rectifier state with P = -600 MW						
IGCT	6422	4024	2183	215	1558	1322
Press IGBT	7068	4081	2987	0	2312	2386
Module IGBT	9137	6720	2417	0	3131	1920
Press IEGT	8563	4747	3816	0	2281	2955
Module IEGT	8260	5604	2656	0	2755	2109
Inverter state with P = 600 MW						
IGCT	6350	3952	2183	215	1607	1322
Press IGBT	7141	4154	2987	0	2463	2386
Module IGBT	9212	6795	2417	0	3369	1920
Press IEGT	8551	4735	3816	0	2390	2955
Module IEGT	8244	5588	2656	0	2915	2109
Reactive power state with Q = -600 MVar						
IGCT	5537	3362	2022	153	1362	1374
Press IGBT	5998	3389	2609	0	1938	2157
Module IGBT	7686	5523	2163	0	2587	1789
Press IEGT	7235	3955	3280	0	1955	2632
Module IEGT	6894	4568	2326	0	2330	1915
Reactive power state with Q = 600 MVar						
IGCT	5458	3362	1943	153	1362	1029
Press IGBT	6202	3389	2813	0	1938	2175
Module IGBT	7748	5523	2225	0	2587	1697
Press IEGT	7602	3955	3647	0	1955	2733
Module IEGT	7063	4568	2495	0	2330	1915

the FB-MMCs based on press-pack IGBT, module-type IGBT, press-pack IEGT, and module-type IEGT increase the loss by 13.6%, 42.0%, 39.3%, and 29.4%, respectively.

It should be noticed that different with HB-MMC, there are four switches in the FB submodule. However, two couples are symmetrical, so we still use upper and lower switches to describe, when upper switches turn ON, the output voltage of FB is positive and when lower switches turn ON, the output voltage is negative or zero. In addition, because the modulation ratio of FB-MMC can be higher than 1, the reactive power that can generate to power grid for FB-MMC can reach 600 MVar.

B. Comparison of Power Loss with Different Switching Frequencies

Fig. 17 shows the power loss of FB-MMC with different switching frequencies. It can be seen that the power loss of FB-MMC still increases with the increase in the switching frequency. The FB-MMCs based on module-type IGBT and press-pack IEGT still have the highest power loss during all the ranges. However, the range changes to be wider for module-type IGBT than that in HB-MMC. The MMC based on IGCT always has the lowest power loss under all the operation states.

C. Comparison of Power Loss with Different Powers

Fig. 18 shows the power loss of FB-MMC with different powers. It can be seen that the power loss of FB-MMC is higher than that of HB-MMC with the same transmission power. The FB-MMC based on IGCT still has the lowest power loss during all the operation states, and the FB-MMCs

based on module-type IGBT and press-pack IEGT have the highest power loss.

VIII. CONCLUSION

The power loss performance of MMC based on IGCT for HVDC application is analyzed comprehensively in this paper. Especially, the comparison of MMCs based on IGCTs, IGBTs, and IEGTs is discussed in detail. According to the study in this paper, the snubber power loss of MMC based on IGCT is far less than the conduction and switching power losses. If we just consider switches, compared with MMC based on IGBTs and IEGTs, both the upper and lower IGCTs have the lowest power losses during all the operation states of MMC. Moreover, because the turn-ON energy of IGCT is far lower than that of IGBTs and IEGTs, both the conduction and switching power losses of IGCT are lower than that of IGBTs and IEGTs. The power loss reduction of FB-MMC based on IGCT is more significant than that of HB-MMC based on IGCT, because more switches are employed in FB-MMC. If taking diodes into account, the HB-MMC and FB-MMC based on IGCT can decrease power loss about 1.9%–49.3% and 8.3%–45.1% under different operation states, respectively. The study in this paper will provide a valuable reference and promote the application of IGCT in MMC.

REFERENCES

[1] A. Egea-Álvarez, F. Bianchi, O. Gomis-Bellmunt, A. Junyent-Ferre, and G. Gross, "Voltage control of multiterminal VSC-HVDC transmission systems for offshore wind power plants: Design and implementation in a scaled platform," *IEEE Trans. Ind. Electron.*, vol. 60, no. 6, pp. 2381–2391, Jun. 2013.

[2] N. Flourentzou, V. G. Agelidis, and G. D. Demetriades, "VSC-based HVDC power transmission systems: An overview," *IEEE Trans. Power Electron.*, vol. 24, no. 3, pp. 592–602, Mar. 2009.

[3] R. T. Pinto, P. Bauer, S. F. Rodrigues, E. J. Wiggelinkhuizen, J. Pierik, and B. Ferreira, "A novel distributed direct-voltage control strategy for grid integration of offshore wind energy systems through MTDC network," *IEEE Trans. Ind. Electron.*, vol. 60, no. 6, pp. 2429–2441, Jun. 2013.

[4] S. Bernal-Perez, S. Ano-Villalba, R. Blasco-Gimenez, and J. Rodriguez-D'Derlee, "Efficiency and fault ride-through performance of a diode-rectifier- and VSC-inverter-based HVDC link for offshore wind farms," *IEEE Trans. Ind. Electron.*, vol. 60, no. 6, pp. 2401–2409, Jun. 2013.

[5] M. Davari and Y. A.-R. I. Mohamed, "Dynamics and robust control of a grid-connected VSC in multiterminal DC grids considering the instantaneous power of DC- and AC-side filters and DC grid uncertainty," *IEEE Trans. Power Electron.*, vol. 31, no. 3, pp. 1942–1958, Mar. 2016.

[6] H. Rao, "Architecture of Nan'ao multi-terminal VSC-HVDC system and its multi-functional control," *CSEE J. Power Energy Syst.*, vol. 1, no. 1, pp. 9–18, Jan. 2015.

[7] J. Egan, P. O'Rourke, R. Sellick, P. Tomlinson, B. Johnson, and S. Svensson, "Overview of the 500 MW EirGrid East-West Interconnector, considering System Design and execution-phase issues," in *Proc. 48th Int. Univ. Power Eng. Conf. (UPEC)*, Sep. 2013, pp. 1–6.

[8] A. Abdalrahman and E. Isabegovic, "DolWin1—Challenges of connecting offshore wind farms," in *Proc. IEEE Int. Energy Conf. (ENERGYCON)*, Apr. 2016, pp. 1–10.

[9] J. Beerten, G. B. Diaz, S. D'Arco, and J. A. Suul, "Comparison of small-signal dynamics in MMC and two-level VSC HVDC transmission schemes," in *Proc. IEEE Int. Energy Conf. (ENERGYCON)*, Apr. 2016, pp. 1–6.

[10] I. G. Torres, H. Miranda, V. Cardenas, and R. A. Salas, "Gain scheduling scheme assisting the control strategy for three-level NPC VSC-HVDC transmission system," in *Proc. 40th Annu. Conf. IEEE Ind. Electron. Soc. (IECON)*, Oct./Nov. 2014, pp. 4635–4641.

[11] W. Yang, Q. Song, and W. Liu, "Decoupled control of modular multilevel converter based on intermediate controllable voltages," *IEEE Trans. Ind. Electron.*, vol. 63, no. 8, pp. 4695–4706, Aug. 2016.

[12] G. P. Adam, I. A. Abdelsalam, K. H. Ahmed, and B. W. Williams, "Hybrid multilevel converter with cascaded H-bridge cells for HVDC applications: Operating principle and scalability," *IEEE Trans. Power Electron.*, vol. 30, no. 1, pp. 65–77, Jan. 2015.

[13] Q. Song, W. Liu, X. Li, H. Rao, S. Xu, and L. Li, "A steady-state analysis method for a modular multilevel converter," *IEEE Trans. Power Electron.*, vol. 28, no. 8, pp. 3702–3713, Aug. 2013.

[14] J.-J. Jung, S. Cui, J.-H. Lee, and S.-K. Sul, "A new topology of multilevel VSC converter for a hybrid HVDC transmission system," *IEEE Trans. Power Electron.*, vol. 32, no. 6, pp. 4199–4209, Jun. 2017.

[15] P. Bordignon, H. Zhang, W. Shi, N. Serbia, and A. Coffetti, "HV submodule technology based on press pack IGBT for largest scale VSC-HVDC application," in *Proc. 12th IET Int. Conf. AC DC Power Transmiss. (ACDC)*, 2016, pp. 1–6.

[16] H. Wang and K.-W. Ma, "IGBT technology for future high-power VSC-HVDC applications," in *Proc. 12th IET Int. Conf. AC DC Power Transmiss. (ACDC)*, 2016, pp. 1–6.

[17] G. P. Adam and B. W. Williams, "Half- and full-bridge modular multilevel converter models for simulations of full-scale HVDC links and multiterminal DC grids," *IEEE J. Emerg. Sel. Topics Power Electron.*, vol. 2, no. 4, pp. 1089–1108, Dec. 2014.

[18] T. Modeer, S. Norrga, and H.-P. Nee, "Implementation and testing of high-power IGCT-based cascaded-converter cells," in *Proc. IEEE Energy Convers. Congr. Expo. (ECCE)*, Sep. 2014, pp. 5355–5359.

[19] R. Lizana, M. Perez, J. Rodriguez, and B. Wu, "Modular multilevel converter based on current source H-bridge cells implemented with low cost reversing conducting IGCT," in *Proc. IEEE Energy Convers. Congr. Expo. (ECCE)*, Sep. 2013, pp. 3363–3367.

[20] S. Tschirley, S. Bernet, and P. Streit, "Design and characteristics of reverse conducting 10-kV-IGCTs," in *Proc. IEEE Power Electron. Spec. Conf.*, Jun. 2008, pp. 92–97.

[21] P. M. Meshram and V. B. Borghate, "A simplified nearest level control (NLC) voltage balancing method for modular multilevel converter (MMC)," *IEEE Trans. Power Electron.*, vol. 30, no. 1, pp. 450–462, Jan. 2015.

[22] S. Du, J. Liu, and T. Liu, "Modulation and closed-loop-based DC capacitor voltage control for MMC with fundamental switching frequency," *IEEE Trans. Power Electron.*, vol. 30, no. 1, pp. 327–338, Jan. 2015.

[23] P. Ladoux, N. Serbia, and E. I. Carroll, "On the potential of IGCTs in HVDC," *IEEE J. Emerg. Sel. Topics Power Electron.*, vol. 3, no. 3, pp. 780–793, Sep. 2015.

[24] M. Buschendorf, J. Weber, and S. Bernet, "Comparison of IGCT and IGBT for the use in the modular multilevel converter for HVDC applications," in *Proc. Int. Multi-Conf. Syst., Sygnals Devices*, Mar. 2012, pp. 1–6.

[25] I. Etxeberria-Otadui, J. San-Sebastian, U. Viscarret, I. Perez-de-Arenaza, A. Lopez-de-Heredia, and J. M. Azurmendi, "Analysis of IGCT current clamp design for single phase H-bridge converters," in *Proc. IEEE Power Electron. Spec. Conf.*, Jun. 2008, pp. 4343–4348.

[26] S. Singh, "IGCT transient analysis and clamp circuit design for VSC valves," M.S. thesis, Royal Inst. Technol., Stockholm, Sweden, 2012.

Rong Zeng (M'02–SM'06) was born in Shaanxi, China, in 1971. He received the B.Eng., M.Eng., and Ph.D. degrees from the Department of Electrical Engineering, Tsinghua University, Beijing, China, in 1995, 1997, and 1999, respectively.

He is currently a Professor with the Department of Electrical Engineering, Tsinghua University. His current research interests include power semiconductors, dc circuit breakers, and dc transmission and distribution systems.

Jianguo Li was born in Hebei, China, in 1975. He received the B.S. degree from the Department of Electrical Engineering, North China Electric Power University, Beijing, China, in 1997, the M.S. degree from the Department of Electrical Engineering, Tsinghua University, Beijing, in 2005, and the Ph.D. degree from the College of Electrical and Electronic Engineering, North China Electric Power University, Beijing, in 2017.

His current research interests include bidirectional dc–dc converters, high-frequency link power conversion systems, and flexible ac and dc transmission or distribution systems.

Tianyu Wei was born in Dezhou, China, in 1993. He received the B.S. degree from the Department of Electrical Engineering, Tsinghua University, Beijing, China, in 2016, where he is currently pursuing the master's degree.

His current research interests include dc circuit breakers and high-power electronic converters.

Zhengyu Chen was born in Tianjin, China, in 1992. He received the B.S. degree from the Department of Electrical Engineering, Tsinghua University, Beijing, China, in 2014, where he is currently pursuing the Ph.D. degree.

His current research interests include power semiconductor devices and their gate unit drivers, high voltage dc systems, and dc circuit breakers.

Qiang Song (M'14) was born in Changchun, China, in 1975. He received the B.S. and Ph.D. degrees from the Department of Electrical Engineering, Tsinghua University, Beijing, China, in 1998 and 2003, respectively.

He is currently an Associate Professor with the Department of Electrical Engineering, Tsinghua University. His current research interests include high-power electronic interfaces for utility systems, flexible ac transmission systems, and motor drives.

Biao Zhao (S'11–M'14) was born in Hubei, China, in 1987. He received the B.S. degree from the Department of Electrical Engineering, Dalian University of Technology, Dalian, China, in 2009, and the Ph.D. degrees from the Department of Electrical Engineering, Tsinghua University, Beijing, China, in 2014.

He is currently an Assistant Professor with the Department of Electrical Engineering, Tsinghua University. His current research interests include high-power dc–dc converters, power electronic transformers, and flexible dc transmission and distribution systems.

Dr. Zhao is a member of the IEEE Power Electronics Society, the Industrial Electronics Society, and the Chinese Society for Electrical Engineering.
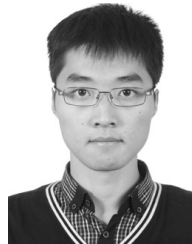
Zhanqing Yu (M'07) was born in Inner Mongolia, China, in 1981. He received the B.Sc. and Ph.D. degrees from the Department of Electrical Engineering, Tsinghua University, Beijing, China, in 2003 and 2008, respectively.

He is currently an Associate Professor with the Department of Electrical Engineering, Tsinghua University. His current research interests include dc circuit breakers, electromagnetic environments and electromagnetic compatibility, and dc transmission and distribution systems.